

## A Model of Social Distancing for Interacting Age-Distributed Multi-Populations: An Analysis of Students' In-Person Return to Schools

A. C. F. N. Gomes<sup>1\*</sup> and A. De Cezaro<sup>2</sup>

Received on March 14, 2021 / Accepted on May 6, 2022

**ABSTRACT.** Because of the current scenario of the SARS-CoV-2 (COVID-19) pandemic in Brazil, whose vaccination campaign is in its initial stage, government authorities have pointed towards the complete reopening of the economy. And recently, for the in-personal return of classroom teaching in schools. Given the family relationship, one of the questions that remains without an answer is: what are the consequences of the schools' reopening on the dissemination of COVID-19? The purpose of this work is to analyze a variant of the compartmental SIRD (Susceptible, Infected, Recovered, Social Distancing) model in a structured, interacting age population representing six age groups, from the basic education age to the elderly. We present a complete analysis of the well-posedness of the proposed mathematical model. We discuss distinct disease spreading scenarios based on observations of the mathematical behavior of the proposed dynamics. Moreover, we present the existence of the stationary points in terms of the parameters of the model and the number of infected age groups. Finally, we present different numerical simulations of the predicted scenarios by the model. Those numerical realizations support the conclusion that an early school reopening, resulting in the decreasing social isolation of young people, causes the infection curve to grow considerably, even for other age groups.

**Keywords:** COVID-19, SARS-CoV-2, SIRQ model, multi-population.

### 1 INTRODUCTION

The SARS-CoV-2 virus, which causes COVID-19, was first reported in Wuhan (Hubei, China) at the end of 2019. From there it spread rapidly and became a global pandemic [15, 19]. This situation, unprecedented in the recent history of humanity, requires a large part of the scientific community's efforts to collect information, generate, and test evidence that allows us to plan and execute prevention, control, and treatment strategies for mitigating the virus' spread. Despite the effort, COVID-19 caused an enormous impact on economic and social behavior, besides millions of deaths related to the pandemic worldwide [12].

---

\*Corresponding author: Ana Carla F. Nicola Gomes – E-mail: anagomes.mat@gmail.com

<sup>1</sup>Institute of Mathematics, Statistics and Physics, Graduate Program in Computational Modeling, Federal University of Rio Grande, Rio Grande, RS, Brazil – E-mail: anagomes.mat@gmail.com <https://orcid.org/0000-0003-2815-1612>

<sup>2</sup>Institute of Mathematics, Statistics and Physics, Federal University of Rio Grande, Rio Grande, RS, Brazil – E-mail: adrianocezaro@furg.br <https://orcid.org/0000-0001-8431-9120>

Historically, mathematical models have proved to be important tools for studying and predicting the dynamics of many epidemics. Such models have been the subject of research since Bernoulli's pioneering work [5]. It was the first model that divided the total population into compartments, [2]. The same importance of mathematical models becomes evident within the turn-over direction of the UK government's decision to prevent the COVID-19 spread [18].

Since COVID-19 has a high level of contagious infection and respiratory complications, it rapidly spreads to a significant rate of hospitalization with high mortality, particularly among those requiring ventilation [17]. In the early stages of the pandemic, many governmental authorities strongly argued in favor of vertical social isolation, maintaining only the most vulnerable (the elderly among them) in social isolation. However, facts as social conditions impose the necessity of inter-generational contact [18], causing the health system capacity limit to collapse.

Therefore, the absence of specific antiviral prophylaxis [1] or vaccines imposes the only remaining alternative to efficaciously control the SARS-CoV-2 virus spread: non-pharmaceutical intervention. That consists of physical distancing measures allied with strategies of person-to-person preventive transmission like wearing a mask, banning collective gatherings [6, 7], among others.

This contribution aims to place a new piece in the puzzle of COVID-19 spread: understanding the effect of the in-personal return of schools on the propagation dynamics of COVID-19 among the population. Even if children are not a high-risk group, as the schools reopen, the transmission of the virus could take place among students, their kin, and school staff [16].

In this scenario, we assume that the dynamics are governed by a variation of the compartmental SIRD (S-susceptible, I-infected or infectious, R-recovered, and D-social distancing) model, with an interacting multi-population divided by age range. As a measure for controlling the spread of the virus (see Section 2 for details), the social distancing compartment is assumed to include voluntarily healthy individuals from each of the social groups considered in the analysis. It is worth mentioning that the proposed and analyzed model is an extension of the approach proposed in [13], including the social distance compartment.

**Main contributions and manuscript organization:** In Section 2, we present the age-interacting compartmental SIR-like multi-population model analyzed in this contribution. We present a complete analysis of the well-posedness of the model in Subsection 2.1. Moreover, we discuss distinct disease spreading scenarios based on observations of the mathematical behavior of the proposed dynamics.

We also present a result of existence for the stationary points in terms of the parameters of the model and the number of infected age groups in Subsection 2.2. In Section 3, we present different numerical simulations of the predicted scenarios by the model. Those numerical realizations collaborate with the conclusion that an early school reopening causes the infection curve to grow considerably, even for other age groups. Finally, in Section 4, we present some conclusions and further directions for this contribution.

## 2 SIRD MODEL FOR AN AGE DISTRIBUTED MULTI-POPULATION INTERACTING

In this contribution, we start from the assumption that we have a constant total population of size  $N_T$ , that is divided into  $n$  age sub-populations of  $N_i$  individuals in each age group  $i$ , such that  $N_T = \sum_{i=1}^n N_i$ . Furthermore, we assume that the interaction dynamics between the compartments of any of the different age groups is governed by the initial value problem (PVI)

$$\begin{aligned} \dot{S}_i(t) &= \mu_i N_i - \mu_i S_i(t) - S_i(t) \sum_{j=1}^n \beta_{ij} I_j(t) - \gamma_i S_i(t) + \theta_i D_i(t) \\ \dot{I}_i(t) &= S_i(t) \sum_{j=1}^n \beta_{ij} I_j(t) - (\mu_i + \alpha_i) I_i(t) \\ \dot{R}_i(t) &= \alpha_i I_i(t) - \mu_i R_i(t) \\ \dot{D}_i(t) &= \gamma_i S_i(t) - (\theta_i + \mu_i) D_i(t), \end{aligned} \quad (2.1)$$

with initial conditions  $(S_i(0), I_i(0), R_i(0), D_i(0))^T \in \mathcal{R}_+^4 := \{(S_i, I_i, R_i, D_i)^T \in \mathcal{R}^4 : S_i \geq 0, I_i \geq 0, R_i \geq 0, D_i \geq 0\}$ , for  $i \in \{1, \dots, n\}$ . The parameters  $\alpha_i > 0$  and  $\gamma_i > 0$  are, respectively, the inverse of the time that individuals stay in the  $I_i$  compartment and the transition rate for social distancing. Parameters  $\beta_{ij} > 0$  are the rate of contact between individuals in the compartments  $S_i$  and  $I_j$ , for all population age groups  $i, j \in \{1, \dots, n\}$ , respectively.  $\theta_i$  represents the rates of individuals leaving the social distance compartment  $D_i$  and  $\mu_i > 0$  represents the mortality/birth rate that are assumed to be the same, for all  $i \in \{1, \dots, n\}$ . We also assume that the number of people  $N_i$  in each age sub-population ( $i$ ) remains constant, for all  $i \in \{1, \dots, n\}$ .

### 2.1 Theoretical analysis

In this subsection, we address some important theoretical results regarding the proposed model. We start with the well-posedness.

**Theorem 2.1 (Well-posedness and consistency).** *Assume that the system (2.1) is such that the initial conditions are in  $\mathcal{R}_+^4$ , for all  $i \in \{1, \dots, n\}$ . Then there exists a unique solution  $u_i := (S_i, I_i, R_i, Q_i)^T \in C^1([0, \infty[, \mathcal{R}_+^4)$ , for all  $i \in \{1, \dots, n\}$ , which depends continuously on the initial data and parameters of the model.*

**Proof.** The existence of a unique solution in a bounded interval follows from the Lipschitz continuity of the Jacobean on the right-hand side of (2.1) and the classical results on ODE's, e.g., [8]. Since the total population is constant, it follows that each solution coordinate is uniformly bounded. This means that the solution can be extended to  $[0, +\infty[$ , since the right-hand side satisfies the Carathéodory conditions, e.g., [8]. The consistency of the solutions in  $\mathcal{R}_+^4$  follows from the standard ODE theory results, e.g., [8].  $\square$

Next, we address some interesting conclusions based on the proposed model (2.1).

First, notice that Theorem 2.1 implies in, whenever the initial conditions are non-negative, each coordinate of the unique solution of model (2.1),  $(S_i(t), I_i(t), R_i(t), D_i(t))$ , are non-negative, for

all  $i = 1, \dots, n$ . Since there is no reinfection in the model (2.1), it is reasonable to assume that  $R_i(0) = 0$ . Then, from the third equation in (2.1) and the integrating factor method, we get

$$R_i(t) = \alpha_i \int_0^t e^{\mu_i(s-t)} I_i(s) ds. \quad (2.2)$$

It means that the number of recovered people is proportional to the cumulative number of infected individuals in each age class  $i$ .

Moreover, assuming that the number of susceptible individuals of any age-class maintaining social distance also decreases during the evolution of the epidemic (that is a reasonable hypothesis), i.e.  $\dot{D}_i(t) \leq 0$ , we get as a consequence of the last equation in (2.1) that

$$D_i(t) \geq \frac{\gamma_i}{\mu_i + \theta_i} S_i(t). \quad (2.3)$$

Hence, if the *basic reproduction number*<sup>1</sup> of the population  $i$ ,  $\mathcal{R}_0^i$ , is such that  $\mathcal{R}_0^i > 1$ , then we get that  $I_i(t)$  start increasing, e.g., [9, 10, 11]. So is  $R_i(t)$  from (2.2). Given that the total population  $N_i$  is constant, it follows from the first equation in (2.1) and (2.3) that  $S_i(t)$  is non-increasing. Therefore, for  $t$  large enough  $I_i(t)$  shall be decreasing. In particular,  $I_i(t) < \infty$ , for all  $t \geq 0$ .

Therefore, the above-mentioned properties and the smoothness of  $I_i(t)$  (as a result of the Theorem 2.1), we conclude that the trajectory of the solution for  $I_i(t)$  has a concave hump with extremes in  $I_i(0)$  and  $I_i(\infty) = 0$  (because at the end all the population shall be in  $R_i$  class). Hence,  $I_i(t)$  attains a maximum at a point  $t_p^i \in ]0, +\infty[$ , known as the turning point. Assume that at this point of maximum  $I_i(t_p^i) \neq 0$  for all  $i \in \{1, \dots, n\}$  (that is true if  $I_i(0) > 0$  as a consequence of the above discussed properties). From the maximality of  $t_p^i$  and the smoothness of  $I_i(t)$ , we have  $\dot{I}_i(t_p^i) = 0$ . Consequently, it follows from the second equation in (2.1) that

$$S_i(t_p^i) = \frac{(\mu_i + \alpha_i)}{\beta_{ii}} \left( \frac{1}{1 + \sum_{j \neq i}^n \frac{\beta_{ij} I_j(t_p^i)}{\beta_{ii} I_i(t_p^i)}} \right), \quad \text{for } i \in \{1, \dots, n\}. \quad (2.4)$$

The analysis of equation (2.4) reveals some scenarios whose consequences are worth exploring:

- i) If there is no interaction between the different age groups, that is, if  $\beta_{ij} = 0$  for all  $j \neq i$ , then the number of susceptible at the moment  $t_p^i$  is given by  $S_i(t_p^i) = \frac{(\mu_i + \alpha_i)}{\beta_{ii}}$ , for any  $i = 1, \dots, n$ .
- ii) On the other hand, if there is interaction between distinct age populations ( that means  $\beta_{ij} \neq 0$  for  $j \neq i$ ),  $S_i(t_p^i)$  decrease (since the denominator in (2.4) increases), and therefore  $I_i(t_p^i)$  increases.

<sup>1</sup>The quantity that express the expected number of cases directly generated by one case in a population and withing the selected population, at the initial phase of the infection [9, 10, 11].

- iii) It follows from i) and ii) that the only way to keep  $S_i(t_p^i)$  at its highest possible value is the scenario where there is no interaction between populations. Therefore, no matter the reopening of schools, it will imply an increase in the number of infected cases.
- iv) Assume the scenario where the in-personal returns of school are such that, a few days a week, a proportion of students return to class and stay home the rest of the week. In this situation, we can expect that the parameter  $\beta_{ii}$  of the specific population will increase (considering the greater probability of contact with an infected person). On the other hand, the fact that students stay home a few days a week, makes the interaction with family members (in general with elderly people) also increase proportionately, thereby the term in the denominator of (2.4) is bigger than 1. As a consequence, the number of infected people increases.
- v) Finally, it follows from (2.3 and from (2.4) that  $D_i(t_p^i)$  also decreases with respect to the number of interactions with other populations  $j \neq i$  (that is, with  $\beta_{ij} \neq 0$ ).

The above-mentioned scenarios will be numerically addressed in Section 3. In particular, item i) and ii) corresponds the simulations in Figure (2) and Figure (3), respectively. Item iii) corresponds to Figure (4), Figure (5) and Figure (6).

### 2.2 Existence of equilibrium points

In this subsection, we present the existence of equilibrium points for the model (2.1). It is interesting to note that such equilibrium points depend on the model parameters as well as the interaction between distinct age populations.

It follows from (2.2) that it is enough to analyze the existence of the equilibrium points  $(S_i^*, I_i^*, D_i^*)$  for the reduced model, which consists of the first, second, and fourth equation in (2.1).

From the fourth equation we get:

$$D_i^* = \frac{\gamma_i}{\theta_i + \mu_i} S_i^*. \tag{2.5}$$

Replacing (2.5) in the first equations of the model (2.1) and isolating  $S_i^*$ , we get

$$S_i^* = \frac{\mu_i N_i (\theta_i + \mu_i)}{(\theta_i + \mu_i)(\mu_i + \gamma_i) - \theta_i \gamma_i + (\theta_i + \mu_i) \sum_{j=1}^n \beta_{ij} I_j^*}. \tag{2.6}$$

Finally, by substituting (2.6) in the model's (2.1) second equations, we conclude that any equilibrium  $I_i^*$  is given by the roots of the second-degree polynomial,

$$(I_i^*)^2 + bI_i^* + c = 0, \tag{2.7}$$

where

$$b = \frac{\mu_i}{\beta_{ii}} \left[ 1 - \frac{\beta_{ii} N_i}{(\alpha_i + \mu_i)} + \frac{\gamma_i}{(\theta_i + \mu_i)} \right] + \left( \frac{1}{\alpha_i + \mu_i} \right) \sum_{j=1, j \neq i}^n \frac{\beta_{ij}}{\beta_{ii}} I_j^*$$

and

$$c = -\frac{\mu_i N_i}{(\alpha_i + \mu_i)} \sum_{j=1, j \neq i}^n \frac{\beta_{ij}}{\beta_{ii}} I_j^*$$

Given that we are analyzing a situation that resembles the real-life scenario in which model’s (2.1) initial conditions for the are positive, and thus the model’s (2.1) solution is also positive from Theorem 2.1, it follows that the equilibrium points  $I_i^*$  are the non-negative roots of (2.7). In this context, we have:

**Theorem 2.2 (Existence of equilibrium points).** *Let the initial conditions for the model (2.1) be non-negative. Then there are four possible non-negative roots for (2.7). They are:*

- i) *disease-free equilibrium point  $I_i^* = 0$ , for all  $i \in \{1, \dots, n\}$ .*
- ii)  *$I_i^* = \frac{\mu_i}{\beta_{ii}} \left[ 1 - \frac{\beta_{ii} N_i}{(\alpha_i + \mu_i)} + \frac{\gamma_i}{(\theta_i + \mu_i)} \right]$ , subject to  $\beta_{ij} = 0$  for  $j \neq i$  and  $b > 0$ .*
- iii) *Whenever  $c \neq 0$  and  $b > 0$ , then we have  $I_i^* = \frac{-b + \sqrt{b^2 - 4c}}{2}$ .*
- iv) *Whenever  $c \neq 0$  and  $b < 0$ , then we have  $I_i^* = \frac{-b + \sqrt{b^2 - 4c}}{2}$ .*

**Proof.** Given the assumptions, Theorem 2.1 implies that the number of infected individuals in any  $i$ -age sub-population is non-negative. Since all the parameters in the model( 2.1) are positive, it follows that  $c \leq 0$ . Hence  $b^2 - 4c \geq 0$ . Implying the existence of non-negative roots for (2.7).

Assume that  $\beta_{ij} = 0$  for all  $j \neq i$ . Therefore, we are in the scenario that  $c = 0$ . Hence, it follows that the possible roots of (2.7) satisfies  $I_i^* = 0$  and the assertion i) is proved, or  $I_i^* = b$ . Therefore,  $b$  shall be positive as assumed. Since  $\beta_{i,j} = 0$  for all  $j \neq i$ , it follows that  $I_i^* = \frac{\mu_i}{\beta_{ii}} \left[ 1 - \frac{\beta_{ii} N_i}{(\alpha_i + \mu_i)} + \frac{\gamma_i}{(\theta_i + \mu_i)} \right]$ , and then the assertion ii) is concluded.

Now, assertions iii) and iv) follow directly from  $c \neq 0$  and the signal of  $b$ . □

The assertions in the Theorem 2.2 deserve some remarks.

- The assumption of  $c = 0$  used to derive the assertions i)–ii) in the Theorem 2.2 implies that all neighborhood age populations  $j \neq i$  are free of infection ( $I_j^* = 0$  for any  $j \neq i$ ), and thus we have the disease-free equilibrium point. Or, alternatively,  $\beta_{ij} = 0$  hence, there is no interaction between distinct age populations.
- For the free equilibrium point  $I_i^* = 0$  as in Theorem 2.2 assertion i), it follows from (2.5) and (2.6) that

$$S_i^* = \frac{\theta_i + \mu_i}{\theta_i + \gamma_i + \mu_i} N_i \quad D_i^* = \frac{\gamma_i}{\theta_i + \gamma_i + \mu_i} N_i,$$

resulting in  $D_i^* + S_i^* = N_i$ , as expected.

- Assuming a non-interaction aging populations, i.e., with  $\beta_{ij} = 0$  for all  $j \neq i$  and Theorem 2.2 assertion ii) holds, then

$$\zeta_i := 1 - \frac{\beta_{ii}}{\alpha_i + \mu_i} N_i + \frac{\gamma_i}{\theta_i + \mu_i} > 0.$$

Note that, in this scenario  $I_i^* = \frac{\mu_i}{\beta_{ii}} \zeta_i$ .

- Since  $c \neq 0$ , assertions iii) and iv) in Theorem 2.2 holds true when the disease is active in at least one aging population  $j \neq i$ . In particular, assertion iii) holds when

$$\sum_{j=1, j \neq i}^n \frac{\beta_{ij}}{\beta_{ii}} I_j^* > \frac{\mu_i(\alpha_i + \mu_i)}{\beta_{ii}} \left[ \frac{\beta_{ii}}{(\alpha_i + \mu_i)} N_i - 1 - \frac{\gamma_i}{(\theta_i + \mu_i)} \right],$$

and hence, the number of infected neighborhoods is under-bounded. On the other hand, if assertion iv) holds, then the number of infected neighborhoods has an upper-bound, i.e.,

$$\sum_{j=1, j \neq i}^n \frac{\beta_{ij}}{\beta_{ii}} I_j^* < \frac{\mu_i(\alpha_i + \mu_i)}{\beta_{ii}} \left[ 1 - \frac{\beta_{ii}}{(\alpha_i + \mu_i)} N_i + \frac{\gamma_i}{(\theta_i + \mu_i)} \right].$$

The stability analysis of the stationary points obtained in the Theorem 2.2 will be addressed in future contributions.

### 3 NUMERICAL RESULTS AND DISCUSSION

In this section, we will investigate with some simulations and discussions the in-personal returns to schools in the current scenario where the COVID-19 transmission is still active in many countries, in particular in Brazil. In this contribution, we do not intend to compare the simulated scenarios with any kind of real data, whether it is available or not.

It is well known what has been going on since March of 2020 in Brazil. However, we investigate a simplification of this scenario by assuming that there are infected individuals and that in the whole population the virus is transmissible. Moreover, the opening of schools coincides with the time  $t = 0$ . Although we recognize that this is not a realistic scenario, it can still demonstrate quantitatively the impact of age group interaction.

We assume that the whole population is divided by age as follows: Kindergarten (aging from 0 to 5 years old) corresponds to the  $i = 1$  sub-population; primary school I (aging from 6 to 10 years old) corresponds to the  $i = 2$  sub-population, primary school II (aging from 11 to 14 years old) corresponds to the  $i = 3$  sub-population; secondary school (aging from 15 to 17 years old) corresponds to the  $i = 4$  sub-population; working for the population (aging from 18 to 64 years old) corresponds to the  $i = 5$  sub-population; and the elderly sub-population (age more than 64 years old) corresponds to the  $i = 6$  sub-population. As a result, the system (2.1) will be numerically implemented with  $n = 6$ . In all the numerical experiments presented in this section, the solution of (2.1) is approximated by a Runge-Kutta type strategy<sup>2</sup> [3], with step-size  $h = 10^{-1}$ .

---

<sup>2</sup>We have used the ODE45 in MATLAB.

First setup: In this setup, we assume that all the sup-populations are identical <sup>3</sup>, i.e.,  $N_i = \frac{N_T}{6}$ . The parameters  $\mu_i = 0.01$  (this assumption shall be interpreted as that there is no loss of individuals in each sup-population),  $\alpha_i = 0.07$  and  $\theta_i = 0.5$ , for  $i = 1, \dots, 6$ . The infection rates  $\beta_{ii}$  are the same of the ones considered in [14], given, respectively, by  $\beta_{11} = \beta_{22} = \beta_{33} = \beta_{44} = \beta_{55} = \beta_{66} = 0.59$ . The rates  $\beta_{ij}$  for  $j \neq i$  are chosen according to the age difference, i.e.,  $\beta_{12} = \beta_{21} = \beta_{23} = \beta_{32} = \beta_{34} = \beta_{43} = \beta_{45} = \beta_{54} = \beta_{56} = \beta_{65} = 0.59/2$ ;  $\beta_{13} = \beta_{24} = \beta_{31} = \beta_{35} = \beta_{42} = \beta_{46} = \beta_{53} = \beta_{64} = 0.59/3$ ,  $\beta_{14} = \beta_{25} = \beta_{36} = \beta_{41} = \beta_{52} = \beta_{63} = 0.59/4$ ,  $\beta_{15} = \beta_{26} = \beta_{51} = \beta_{26} = 0.59/5$  and  $\beta_{16} = \beta_{61} = 0.59/6$ .

For simplicity, we assume that the working population is the one that starts with a proportion of individuals infected. It is reflected in the initial conditions given by

$$\begin{aligned} \vec{S}(0) &= \frac{\vec{1}}{6} - \vec{I}(0) - \vec{D}(0) \\ \vec{I}(0) &= (0, 0, 0, 0, 0.01, 0)^T \\ \vec{R}(0) &= \vec{0} \\ \vec{D}(0) &= (0.0688, 0.0688, 0.0768, 0.0768, 0.0272, 0.064)^T, \end{aligned} \tag{3.1}$$

where,  $\vec{S}(0) = (S_1(0), S_2(0), S_3(0), S_4(0), S_5(0), S_6(0))^T$ ,  $\frac{\vec{1}}{6}$  is a vector with all the coordinates constants and equal to  $\frac{1}{6}$ ,  $\vec{I}(0) = (I_1(0), I_2(0), I_3(0), I_4(0), I_5(0), I_6(0))^T$ ,  $\vec{R}(0) = (R_1(0), R_2(0), R_3(0), R_4(0), R_5(0), R_6(0))^T$ ,  $\vec{0}$  is the null vector and  $\vec{D}(0) = (D_1(0), D_2(0), D_3(0), D_4(0), D_5(0), D_6(0))^T$ , respectively.

The initial conditions (3.1) do not proportionally reflect the population behavior patterns of the Brazilian state of Rio Grande do Sul, as can be collected from the Epicovid19 data set [4]. On the other hand, the patterns of social distancing and routine activities of the aging groups are described by the parameters  $\gamma_i$ , for  $i = 1, \dots, 6$ . Groups between 20 and 59 years old report being less isolated or reporting going out every day, while other aging groups seem to be well protected, staying at home all day or going out just for essentials, e.g., [4]. Hence, in the simulation we consider  $\gamma_1 = \gamma_2 = \gamma_6 = 0.4$ ,  $\gamma_3 = \gamma_4 = 0.3$  and  $\gamma_5 = 0.1$ .

Figure 1 depicts the dynamic of each compartment of the  $i$  sup-populations for  $i = 1 \dots, 6$  (corresponding to the sub-populations that interact at schools during a reopening). Because the infection rate  $\beta_{ii}$  and the contact rate  $\beta_{ij}$  are assumed to be symmetric, we can see that the behavioral dynamics of each compartment in those sub-populations  $i = 1, \dots, 4$  are nearly the same (which is consistent with the results in Theorem 2.1). In the dynamics of the working and elderly population, we can see how the social distancing classes  $D_5(t)$  and  $D_6(t)$  have different behaviors. The working population does not maintain a social distance, while the elderly population is the one that most manages to maintain it. The similarity of behavior is due to the fact that in our simulations, the parameter choices are similar.

<sup>3</sup>Identical sized sup-populations may appear unrealistic, but this is mitigated in part by the fact that the infection rate ( $\beta_{ii}$ ) is the same for all  $i = 1, \dots, 6$ .

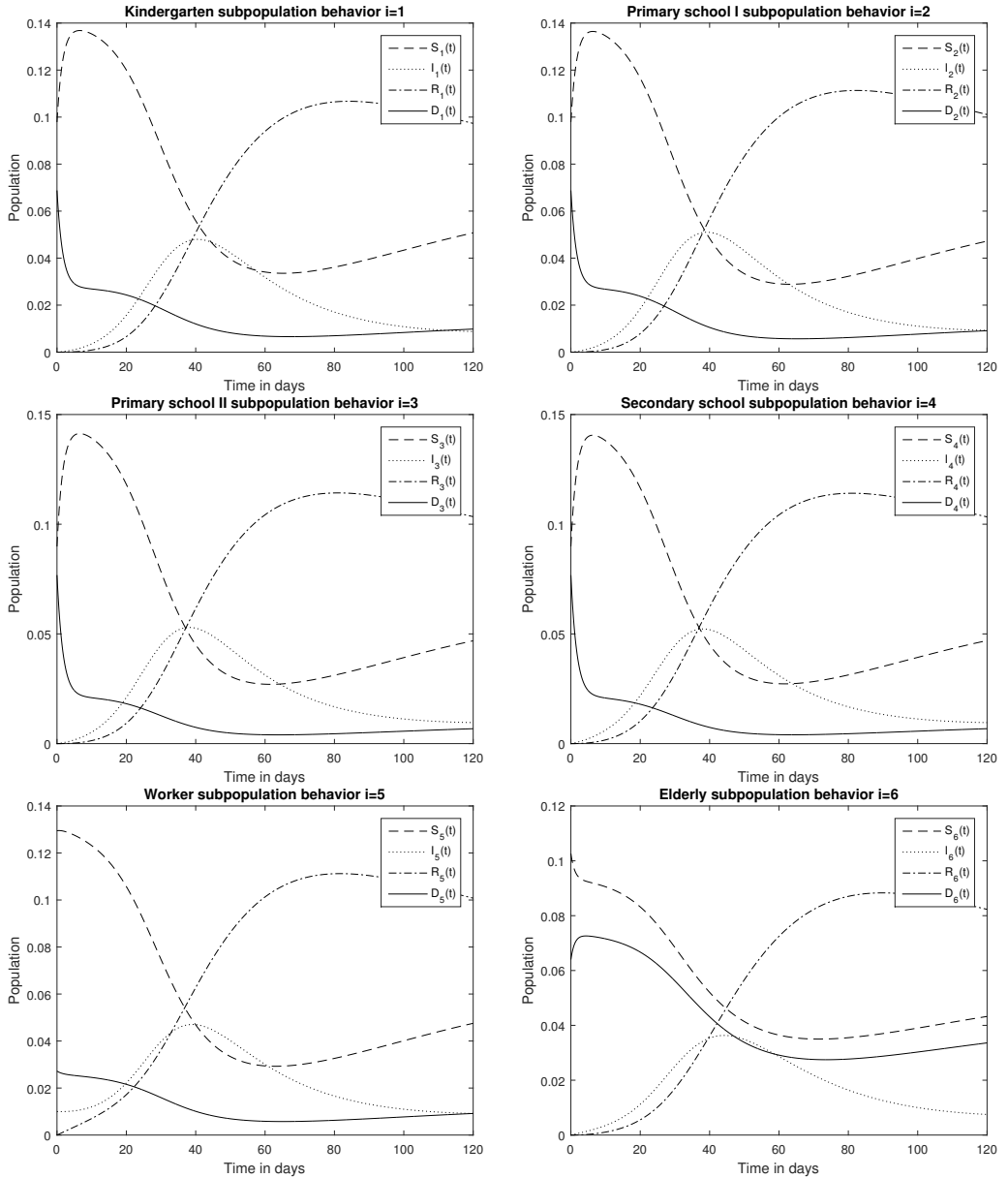


Figure 1: Dynamic of each compartment of the  $i$  sub-populations for  $i = 1 \dots ,6$ , with initial conditions and parameters as in the first setup.

The dynamics of the total population  $S(t) = \sum_{i=1}^6 S_i(t)$ ,  $I(t) = \sum_{i=1}^6 I_i(t)$ ,  $R(t) = \sum_{i=1}^6 R_i(t)$  and  $D(t) = \sum_{i=1}^6 D_i(t)$ , are shown in Figure 2, with the parameters and initial condition presented in the first setup. As shown in Figure 2, there is a rapid decrease in the compartment  $D$ , followed by a transition to the compartment  $S$ , and then an increase in the infected population  $I$ .

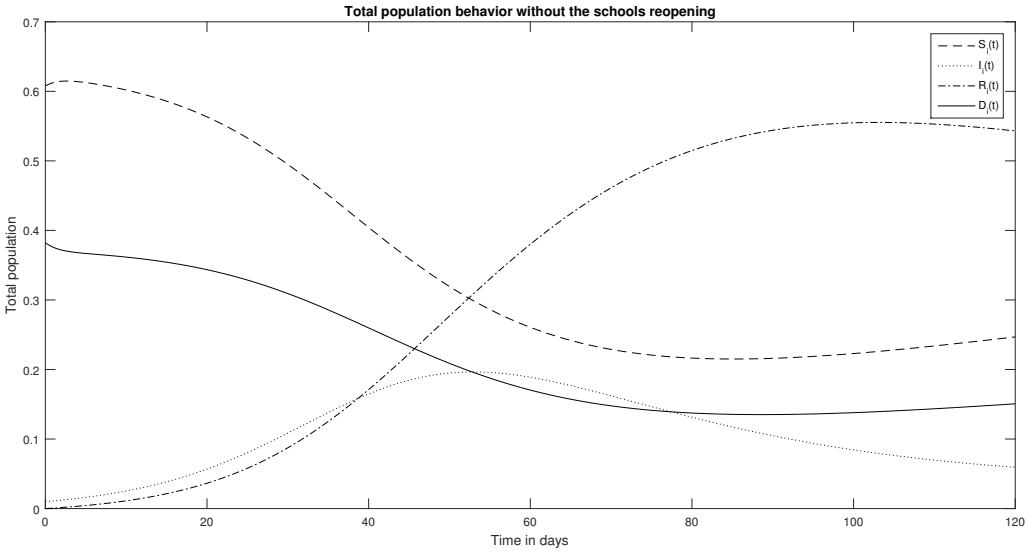


Figure 2: The behavior of the total population without the schools reopening.

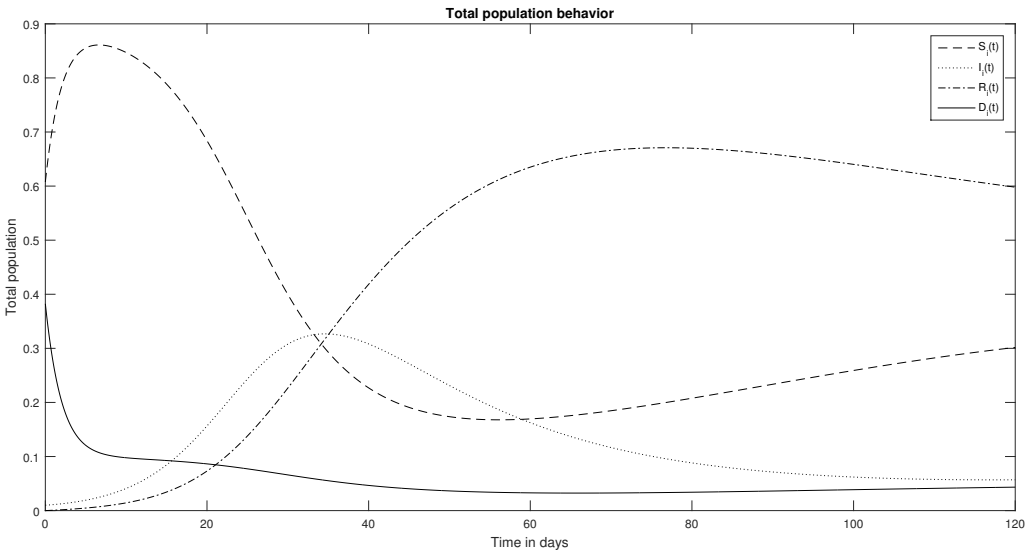


Figure 3: The behavior of the total population with the schools reopening. Simulated scenario with the new set of parameters  $\gamma_1 = \gamma_2 = \gamma_3 = \gamma_4 = 0$  and  $\gamma_5 = 0.1$  and  $\gamma_6 = 0.4$  that corresponds to a relaxation on the social distance proportion of the population  $D_i$ , respectively.

First setup (with schools reopening strategies): In the simulations that follow, we change the parameter  $\gamma_i$ , for  $i = 1, \dots, 4$  that corresponds to a relaxation in the population’s social distance proportion  $D_i$  that mimics scenarios where the schools are reopened, while the remaining parameters and initial conditions are kipped as in the first setup.

Figure 3 shows the dynamics behavior of the total population  $S(t) = \sum_{i=1}^6 S_i(t)$ ,  $I(t) = \sum_{i=1}^6 I_i(t)$ ,  $R(t) = \sum_{i=1}^6 R_i(t)$  and  $D(t) = \sum_{i=1}^6 D_i(t)$ , where  $\gamma_1 = \gamma_2 = \gamma_3 = \gamma_4 = 0$ .

When comparing the dynamical behaviors in the scenario with reopening schools in Figure 3 to the one with constant social distance in Figure 2, it is possible to see drops in the total population in social distancing (compartments  $D_i$ ) and corresponding increases in the susceptible proportion of the population (compartments  $S_i$ ), as well as a significant increase in the proportion of the infected population (compartments  $I_i$ ). Furthermore, there is a shift in the infection peak.

In Figure 4 we present the dynamics of the proportional of the total infected population in a scenario where schools are reopened in a staggered way. We use the following scenario: First, only the kindergarten students attend school (this corresponds to setting  $\gamma_1 = 0$  while the remaining parameters remain fixed as shown in the first setup). Then, the primary school I students attend (which corresponds to taking  $\gamma_1 = \gamma_2 = 0$  while holding the other parameters as in the first setup). Then, the primary school II also goes to school (it corresponds to taking  $\gamma_i = 0$  for  $i = 1, 2, 3$  while the remaining parameters are kept as the ones presented in the first setup). Finally, secondary school students also attend school (it corresponds to taking  $\gamma_i = 0$  for  $i \leq 4$  while the remaining parameters are kept fixed as the ones presented in the first setup). As it can be seen in Figure 4, the total proportion of the population infected is monotonically increasing within the staggered school reopening.

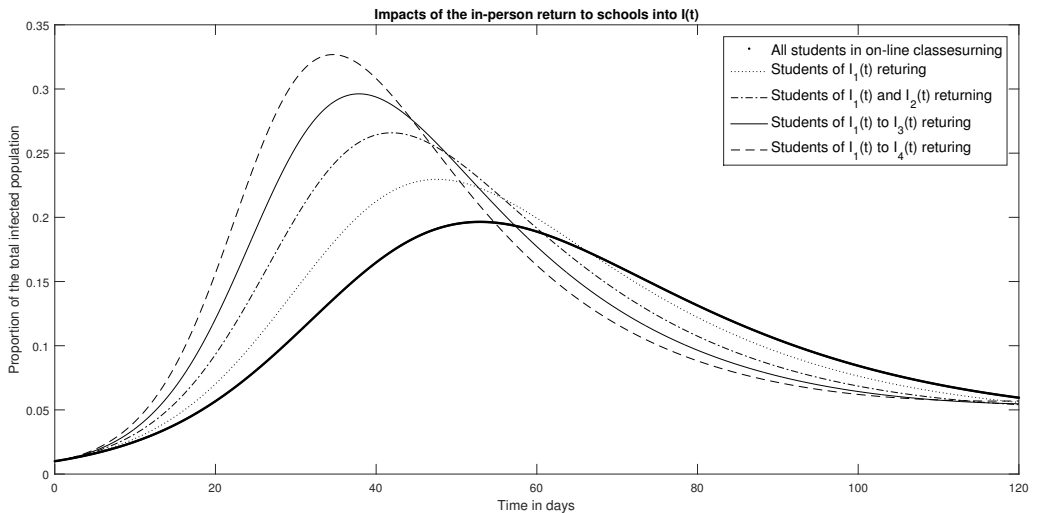


Figure 4: The behavior of the  $I(t) = \sum_{i=1}^6 I_i(t)$  population with the schools staggered reopening.

In Figure 5, we show the evolution of the elder’s infection proportion of the population ( compartment  $I_6$  in the model (2.1)) in the scenario of staggered school reopening discussed above. Notice that its dynamics are also monotonically increasing within the staggered school reopening due to the "in-home" contact with the school-age population as proposed by the analyzed model (2.1).

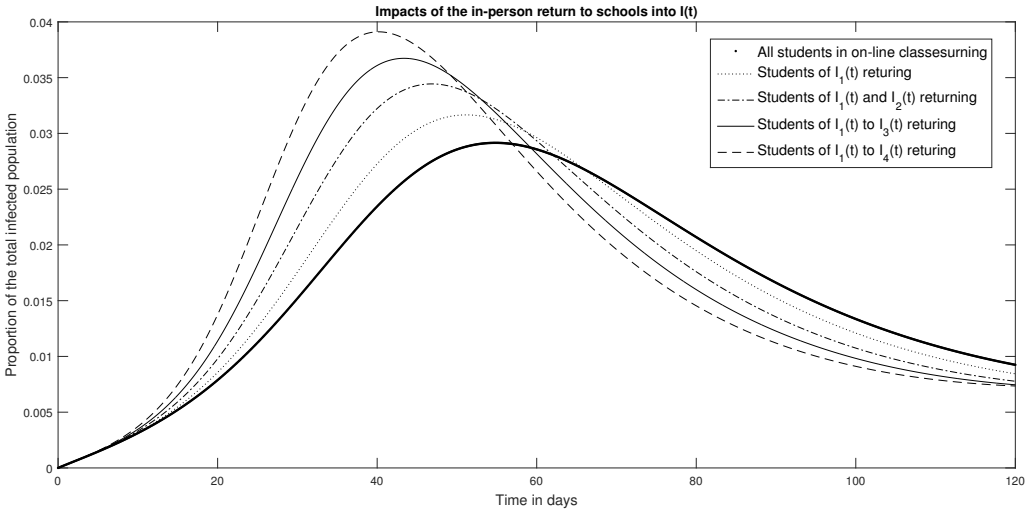


Figure 5: The proportion of the infected people in the elderly population (compartment  $I_6(t)$  dynamics) with the scenario of staggered school reopening.

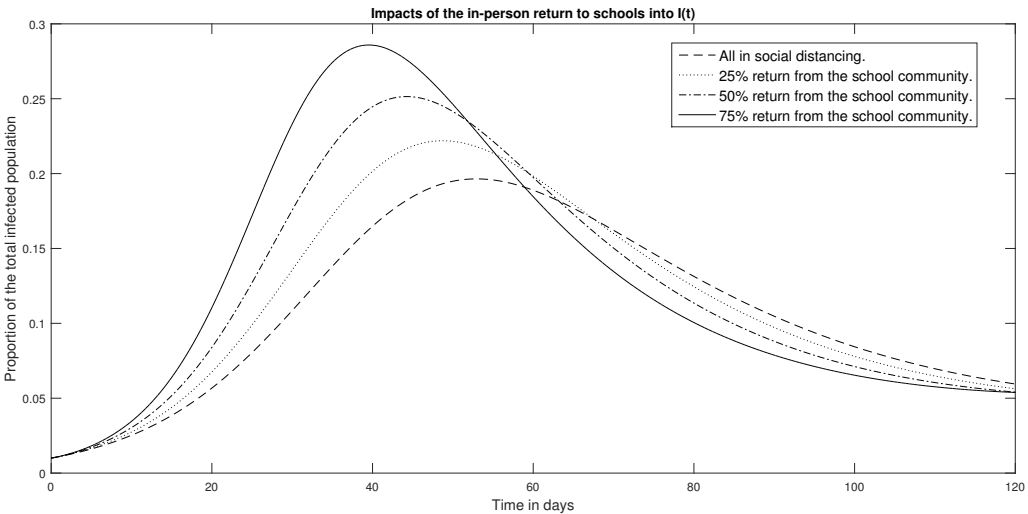


Figure 6: Dynamics of the total infected curve  $I(t) = \sum_{i=1}^6 I_i(t)$  with the scenario of social distancing and the staggered school reopening with 25, 50, and 75 % of occupation capacity.

Next, we show a scenario of the partial return of students to school. Figure 6 presents the effect on the total infected curves of the school community’s considering a partial in-personal return with 25 %, 50 %, and 75 % of its population. For the simulations only change the parameters  $\gamma_i$ , respectively by,  $\gamma_1 = \gamma_2 = 0.3$  and  $\gamma_3 = \gamma_4 = 0.225$  for the scenario of 25 % of returning;  $\gamma_1 = \gamma_2 = 0.2$  and  $\gamma_3 = \gamma_4 = 0.15$  in the scenario with 50 % returning and  $\gamma_1 = \gamma_2 = 0.1$  and

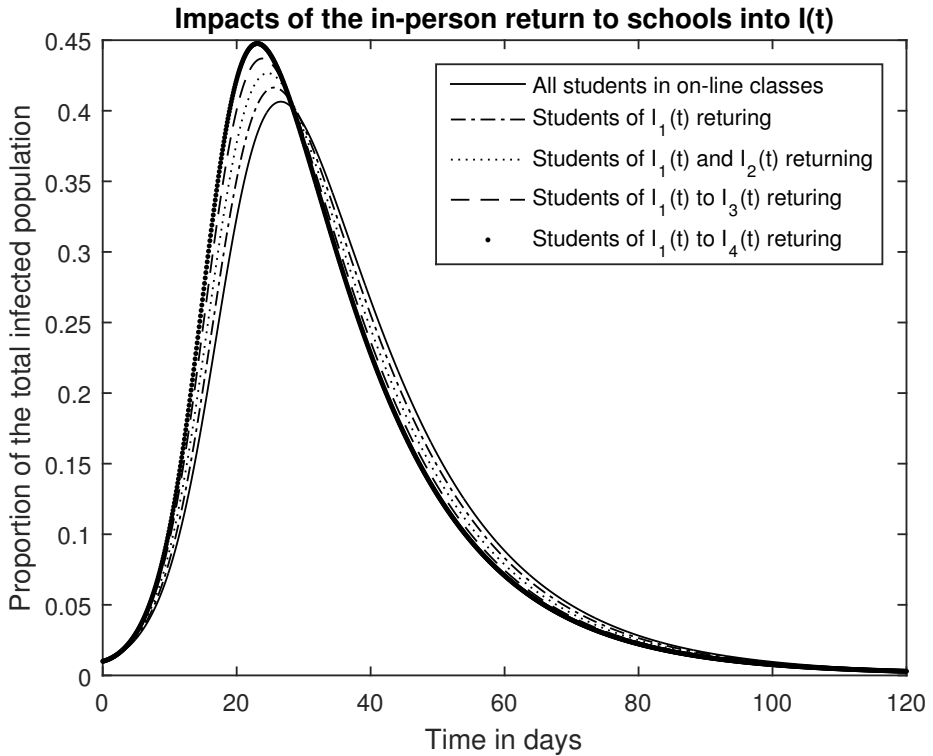


Figure 7: Impact on the total infected population  $I(t)$  due to a staggered in-person return to schools with distinct sub-population densities.

$\gamma_3 = \gamma_4 = 0.075$  for the scenario with a return to 75 % of the school community, while the remaining parameters and initial conditions are the same as the ones presented in the first setup.

It follows from the simulations in Figure 6 that, even in the scenario 25% of the in-personal school returning, there are 20 % of the infected population at the peak of infection.

Second setup: We assume that the densities of sub-populations are such that  $N_1 = N_2 = N_3 = N_4 = 0.08N_T$ ,  $N_5 = 0.48N_T$  and  $N_6 = 0.2N_T$ . The parameters  $\{\mu_i, \alpha_i, \theta_i\}_{i=1}^6$  are the same as in the first setup, and  $\gamma_i$  are chosen as in the first setup with schools' reopening strategies.

The infection rates in each sub-populations are given by  $\beta_{11} = \beta_{22} = \beta_{33} = \beta_{44} = 0.3$ ,  $\beta_{55} = 0.2$  and  $\beta_{66} = 0.1$ . The infection rates between distinct sub-populations are chosen following the idea that: closed aging at school sub-populations have a higher probability of getting together, hence  $\beta_{12} = \beta_{21} = \beta_{23} = \beta_{32} = \beta_{34} = \beta_{43} = 0.3/2$ ,  $\beta_{13} = \beta_{31} = \beta_{24} = \beta_{42} = \beta_{14} = \beta_{41} = 0.1$ ; the interaction between at-school sub-populations and the working class (where fathers belong) is higher than other inter-interactions such that  $\beta_{15} = \beta_{51} = \beta_{25} = \beta_{52} = \beta_{35} = \beta_{53} = \beta_{45} = \beta_{54} = 0.7$ ; young people interact with the elderly more than adolescents, hence  $\beta_{16} = \beta_{61} = \beta_{26} = \beta_{62} =$

0.5,  $\beta_{36} = \beta_{63} = \beta_{46} = \beta_{64} = 0.3$ , and finely, the interaction between the working aging group and elderly are assumed to be  $\beta_{56} = \beta_{65} = 0.3$

The initial conditions are

$$\begin{aligned}\vec{S}(0) &= (N_1, N_2, N_3, N_4, N_5, N_6)^T - \vec{I}(0) - \vec{D}(0) \\ \vec{I}(0) &= (0, 0, 0, 0, 0.01, 0)^T, \quad \vec{R}(0) = \vec{0} \\ \vec{D}(0) &= (0.65N_1, 0.65N_2, 0.5N_3, 0.5N_4, 0.25N_5, 0.65N_6)^T,\end{aligned}\tag{3.2}$$

implying that the diseases starts in the working sub-population. Here,  $\vec{S}(0), \vec{I}, \vec{R}(0), \vec{D}(0)$  have the same meaning as in the first setup.

Figure 7 depicts the effect of staggered return of students to schools of each age group  $i = 1, \dots, 4$ , on the total infected population. Figure 8 shows the effect of the in-personal return to schools of each aging sub-population in the infected on each sub-population, respectively.

Figures 7-8 show that the gradually increasing number of people returning to schools in each sub-population implies a monotonically increasing effect in the infected population and, respectively, in the sub-population, with the peak of infection ranging from 20 to 40 days before schools reopen.

It follows from the simulations presented above that school re-openings should be considered with care.

#### 4 CONCLUSIONS AND FUTURE DIRECTIONS

The results presented in this contribution illustrate the potential impact of the social distancing relaxing of the courses of the COVID-19 pandemic. Our findings show that even partial relaxations in this important non-pharmaceutical intervention, such as partial school reopening, considerably increase the proportional number of infected people. It also shows that a vertical social distancing strategy defended by some governmental authorities might have a devastating impact on the more vulnerable classes, given the inter-aging social interaction.

Moreover, the simulated scenarios show that, in a country like Brazil, where inter-generational contact is very large, even the release of the most distant age group of the elderly causes the infection curve of the elderly to increase. Since the elderly are, by now, most vulnerable in the sense that COVID-19 has dangerous consequences, such school returning might imply an increasing mortality rate among them. Therefore, school re-openings should be considered with care.

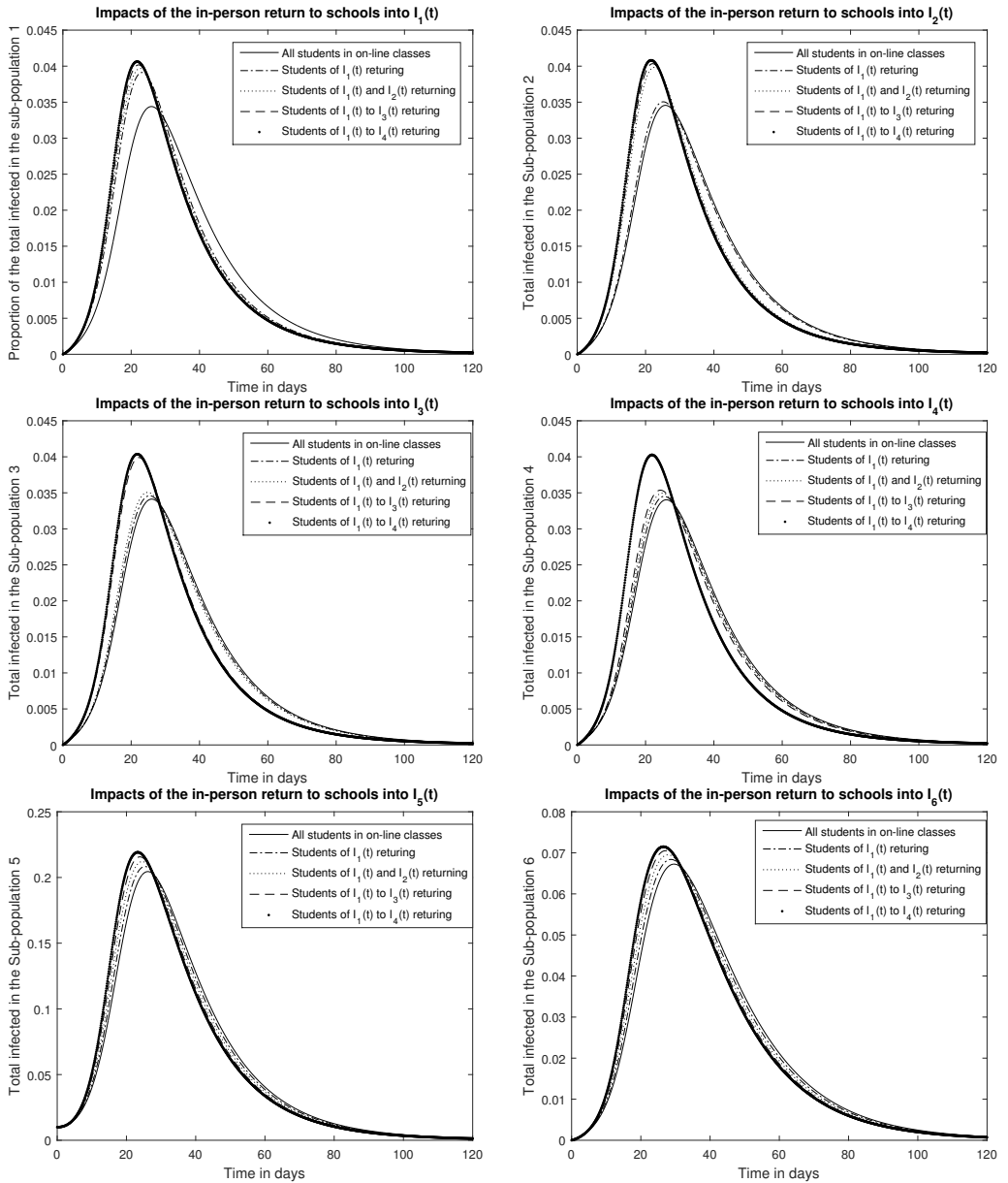


Figure 8: Impact of a staggered in-person return to schools in the infected sub-population  $I_i(t)$ ,  $i = 1, \dots, 6$ , with distinct sub-population densities.

Our next steps regarding the approach presented in this contribution will be:

- Derive the full stability analysis for the model (2.1).
- Simulate numerical scenarios for parameter choices that satisfy the assertions of Theorem 2.2.
- Analyze more numerical scenarios with distinct population densities and parameters that simulate distinct school reopening strategies.
- Extend the model and analysis to include time-dependent parameters.
- Calibrate the model parameters using real data.

### Acknowledgments

This work was supported in part by CNPq and FAPERGS, Brazilian funding agencies and PPGMC-FURG.

### REFERENCES

- [1] A. Aleta *et al.* Modelling the impact of testing, contact tracing and household quarantine on second waves of COVID-19. *Nature Human Behaviour*, **4**(9) (2020), 964–971.
- [2] R. Anderson & R. May. Vaccination against rubella and measles: quantitative investigations of different policies. *Epidemiology & Infection*, **90**(2) (1983), 259–325.
- [3] U.M. Ascher & L.R. Petzold. “Computer Methods for Ordinary Differential Equations and Differential-Algebraic Equations”, volume 1. SIAM (1998).
- [4] A.J. Barros *et al.* Padrões de distanciamento social em nove cidades gaúchas: estudo Epicovid19/RS. *Revista de Saúde Pública*, **54** (2020), 75.
- [5] D. Bernoulli. Essai d’une nouvelle analyse de la mortalité causée par la petite vérole, et des avantages de l’inoculation pour la prévenir. *Histoire de l’Acad., Roy. Sci.(Paris) avec Mem.* (1760), 1–45.
- [6] J.M. Brauner *et al.* Inferring the effectiveness of government interventions against COVID-19. *Science*, **371**(6531) (2021).
- [7] D.K. Chu *et al.* Physical distancing, face masks, and eye protection to prevent person-to-person transmission of SARS-CoV-2 and COVID-19: a systematic review and meta-analysis. *The Lancet*, **395**(10242) (2020), 1973–1987.
- [8] J.K. Hale. “Ordinary Differential Equations (2nd ed.)”, volume 1. Malabar: Robert E. Krieger Publishing Company (1980).
- [9] H.W. Hethcote. Three basic epidemiological models. In “Applied mathematical ecology”. Springer (1989), p. 119–144.

- [10] H.W. Hethcote. The mathematics of infectious diseases. *SIAM review*, **42**(4) (2000), 599–653.
- [11] M. Keeling & P. Rohani. “Modeling Infectious Diseases in Humans and Animals.”. Princeton University Press (2007).
- [12] Z. Khan, Y. Karataş & H. Rahman. Anti COVID-19 drugs: need for more clinical evidence and global action. *Advances in therapy*, **37**(6) (2020), 2575–2579.
- [13] M.J. Lazo & A. De Cezaro. Why can we observe a plateau even in an out of control epidemic outbreak? A SEIR model with the interaction of  $n$  distinct populations for Covid-19 in Brazil. *Trends in Computational and Applied Mathematics*, **22**(1) (2021), 109–123.
- [14] O.P. Neto *et al.* Mathematical model of COVID-19 intervention scenarios for São Paulo—Brazil. *Nature Communications*, **12**(1) (2021), 1–13.
- [15] W.H. Organization. WHO Coronavirus Disease (COVID-19) Dashboard. <https://covid19.who.int> 2020/7/29, (2020).
- [16] J. Panovska-Griffiths *et al.* Determining the optimal strategy for reopening schools, the impact of test and trace interventions, and the risk of occurrence of a second COVID-19 epidemic wave in the UK: a modelling study. *The Lancet Child & Adolescent Health*, **4**(11) (2020), 817–827.
- [17] O.T. Ranzani *et al.* Characterisation of the first 250 000 hospital admissions for COVID-19 in Brazil: a retrospective analysis of nationwide data. *The Lancet Respiratory Medicine*, (2021).
- [18] P.G. Walker *et al.* The impact of COVID-19 and strategies for mitigation and suppression in low-and middle-income countries. *Science*, **369**(6502) (2020), 413–422.
- [19] D. Wang *et al.* Clinical characteristics of 138 hospitalized patients with 2019 novel coronavirus–infected pneumonia in Wuhan, China. *Jama*, **323**(11) (2020), 1061–1069.

